Korean J. Chem. Eng., 37(12), 2179-2191 (2020)
DOI: 10.1007/s11814-020-0628-9

pISSN: 0256-1115
eISSN: 1975-7220

Magnetic graphene oxide-biomass activated carbon composite for dye removal

Tan Yan Ying*, Abdul Aziz Abdul Raman*,†, Mustapha Mohammed Bello, and Archina Buthiyappan***

*Department of Chemical Engineering, Faculty of Engineering, University of Malaya, 50603 Kuala Lumpur, Malaysia
**Centre for Dryland Agriculture, Bayero University, P.M.B. 3011, Kano State, Nigeria
(*Received 17 April 2020 • Revised 30 June 2020 • Accepted 7 July 2020*)

Abstract−A magnetic composite was synthesized using palm kernel shell-based activated carbon, graphene oxide (GO) and iron oxide. The morphology, textural properties, magnetic properties, crystal structure and functional groups of the composite were studied. The characterization shows the successful formation of the ternary composite with a high specific surface area (280.39 m^2/g) and abundant surface functional groups. The magnetic properties of the composite indicate a saturation magnetization of 33.72 emu/g, signifying that the composite can be easily separated with an external magnetic field. The performance of the composite was then investigated through the removal of an anionic azo dye, Acid Blue 113, from aqueous solution. The effect of initial pH of the solution, adsorbent dosage and adsorption contact time was studied. The composite achieved an adsorption capacity of 32.2 mg/g and 96.3% dye removal. Effective dye removal was still achieved after five cycles of adsorption-regeneration, with the dye removal of 74% after the fifth cycle. The analyses of adsorption isotherm and kinetics show that the adsorption process fits pseudo-second-order kinetic and Langmuir isotherm models, indicating a monolayer chemisorption process. The excellent adsorption performance and reusability of the composite and its magnetic separability signify its potential as an adsorbent for wastewater treatment.

Keywords: Adsorption, Modified Graphene Oxide, Iron Oxide, Palm Kernel Shell, Acid Blue 113

INTRODUCTION

As the world's population expands exponentially, one of the key global challenges is the pollution of water resources, which is largely caused by industrial activity. Industrial processes produce myriads of pollutants that often end up in water bodies, posing significant threats to public health and the environment. Many pollutants, such as textile dyes, pesticides, pharmaceuticals and personal care products, are widely found in the environment [1]. Textile industries are among the dominant sources of water pollution [2-4], and it has been estimated that approximately 5,000 tons of textile dyes are released into the environment annually [5]. Textile wastewater contains dissolved solids, inorganic and organic chemicals that can be carcinogenic, and can lead to kidney and central nervous system dysfunction [6-8]. Thus, concerted efforts are needed for the abatement of pollution from textile wastewater.

Over the years, many treatment technologies, such as biological process [9], adsorption [10], photocatalytic oxidation [11] and ultrafiltration [12], have been investigated as possible treatment technologies for textile wastewaters. Adsorption is an attractive technology due to its numerous advantages, including low cost, ease of operation and abundance of potential adsorbents [13-15]. To this end, various adsorbents such as graphene oxide [16], surface-modified chitosan [17], polymeric resins [18], waste coffee-grounds [19], coacervated chitosan particles [20], white sugar activated carbon [21], modified spent tea leaves [22] and black sapote seeds activated carbon [23], have been investigated.

Recently, graphene oxide (GO), a carbon-based material, has received considerable interest as a potential adsorbent due to its high specific surface area and the existence of various functional groups, including carboxyl, hydroxyl and epoxy on its surface [24-27]. However, unavoidable agglomeration, stacking during application and difficulty in post-treatment separation hinder the practical application of GO as an adsorbent [28]. Therefore, modification of GO is often necessary to enhance its properties and performance [29]. Consequently, various modifications of GO to address these drawbacks have been reported. Examples of these include the use of natural polymers such as chitosan to enhance its adsorption capacity and stability [30,31], and iron oxide to enhance its separability [32,33]. Ali et al. [34] have provided a critical review on the modifications of graphene, including functionalized graphene, graphene-based composites and their applications in removing pollutants from wastewater.

While the applications of GO-based adsorbents to remove textile dyes have been reported, a review of the literature shows that more efforts are still needed to develop effective adsorbents for the treatment of textile wastewater. Various ternary magnetic graphene oxide adsorbents have been reported recently, such as magnetic graphene oxide/poly(N-vinylimidazole-co-acrylic acid) hydrogel [35], magnetic chitosan/graphene oxide [36], polyamine-modified magnetic graphene oxide [32], magnetic β-cyclodextrin modified graphene oxide [37] and magnetic graphene oxide decorated with persimmon tannins [38].

In this work, we propose the modification of GO by combining it with iron oxide and a low-cost activated carbon derived from palm kernel shell (PKS), producing a ternary composite as a poten-

†To whom correspondence should be addressed.
E-mail: azizraman@um.edu.my

tial adsorbent for dye removal. The rationale here is to exploit the low-cost and excellent properties of the palm kernel shell activated carbon and synergize them with the inherent properties of the GO, while impacting magnetic properties for ease of post-treatment separation. The use of palm kernel shell, which is an agricultural waste, offers a dual benefit that can lower the treatment cost. It is pertinent to point out that recent interest has shifted towards developing activated carbon from low-cost and renewable feedstocks such as agricultural wastes [39]. To evaluate the performance of the developed composite, an azo dye, Acid Blue 113 (AB113), was used as the model textile dye. Azo dyes, such as AB113, are widely used in the textile industry and possess high chemical stability, making them recalcitrant to conventional treatments [40,41].

The developed composite was fully characterized using BET, FTIR, XRD, SEM/EDX and VSM analyses. The performance of the composite in removing AB113 was then evaluated through batch adsorption. Response surface methodology was used to design the experiments and investigate the effect of operational parameters on the adsorption process. An attempt was also made to model the experimental data and provide insights on the possible mechanism of the adsorption of AB113 by the developed composite. The novelty of this study can be seen in the development of a new ternary composite through synergizing the excellent properties of GO, agricultural waste activated carbon and iron oxide, and its application for the removal of recalcitrant dyes. The ternary composite exhibited superior properties and adsorption capacity compared to the individual materials, indicating its potential as an adsorbent for wastewater treatment. Overall, the results presented will contribute towards the ongoing effort in developing adsorbents for wastewater treatment.

MATERIAL AND METHODS

1. Chemicals

PKS was obtained from Pacific Activated Carbon, Malaysia. Graphite powder (<20 μm), hydrogen peroxide (H_2O_2), ferrous chloride tetrahydrate ($FeCl_2{\cdot}4H_2O$), potassium permanganate ($KMnO_4$), acetic acid (CH_3COOH), sulphuric acid (H_2SO_4), iron (III) chloride hexahydrate ($FeCl_3{\cdot}6H_2O$), ethanol (C_2H_5OH), hydrochloric acid (HCl), potassium chloride (KCl), ammonium hydroxide (NH_4OH) and sodium hydroxide (NaOH) were procured from Sigma Aldrich (M) Sdn. Bhd. Acid Blue 113 (AB113) dye was supplied by Merck Sdn. Bhd. Deionized water was used for all samples preparation. All chemicals were used without further purification.

2. Preparation of MGOAC Composite

The magnetic graphene oxide-activated carbon (MGOAC) was synthesized in two steps. GO was synthesized using an enhanced Hummers method, while MGOAC was developed following the co-precipitation method reported by Taher et al. [42] and Sherlala et al. [43]. First, graphite powder (3 g) was mixed into 70 mL of H_2SO_4 (concentrated) and stirred vigorously for 10 min. Then, $KMnO_4$ (9.0 g) was added slowly for an hour. The steps above were carried out in an ice bath to control the mixture temperature. After that, the mixture was stirred for half an hour at 40 °C. Then, 150 mL of deionized water was added and the mixture was heated to 95 °C and stirred for another 15 min. After 15 min, 500 mL of deionized water was added and 15 mL of H_2O_2 was added dropwise to stop the reaction. The resultant solids (GO) were filtered and washed with 10% of HCl solution. The synthesized GO was dried at 70 °C for 48 h and kept in an airtight container.

For the preparation of MGOAC, GO (1.0 g) was dispersed into a mixture containing CH_3COOH (2%) and HCl (5 mL). Sonication of 30 min was done. Then, 1 g of PKS-AC, $FeCl_3{\cdot}6H_2O$ (4.0 g) and $FeCl_2{\cdot}4H_2O$ (2.0 g) were added in the ratio of 2 : 1 and the mixture was sonicated again for another 30 min. The mixture was stirred overnight and then on the next day, 0.1 M of NH_4OH solution was added dropwise at 25 °C to raise the suspension to pH 8.0 and again sonicated for 30 min. After 12 h, an external magnetic field was used to collect the resultant solids (MGOAC). The solids were washed with deionized water and ethanol, and then dried for 24 h at 60 °C.

3. Characterization of the Composite

The specific surface area of MGOAC composite was studied following Brunauer-Emmett-Teller (BET) and Barrett-Joyner-Halenda (BJH) methods. Scanning electron microscopy coupled with energy dispersive X-ray (SEM/EDX) analysis was conducted using FEI Quanta 200 FESEM (software: Microscope XT) which was run in a low vacuum environment to study the morphology and chemical composition of the composite. The surface functional groups of MGOAC before and after adsorption process were investigated through Fourier transformation infrared (FTIR) spectroscopy using a PerkinElmer Spectrometer (Frontier). Vibrating-sample magnetometer (VSM) system version 4.6.0 (Lake Shore 7400 Series) with maximum field, field increment and ramp rate of 8,000 Oe, 200 Oe and 20 Oe/second respectively was used to examine the magnetic properties of the composite. Additionally, X-ray diffraction (XRD) analysis was conducted to investigate the presence of composite crystalline phase using D8 Advance X-Ray Diffractometer - Bruker AXS (software: DIFFRAC^{plus} - EVA) with 40 kV and 40 mA CuK_α assembled monochromated radiation at ambient temperature. The point of zero charge (pH_{pzc}) of the MGOAC was identified using the method reported by Bach et al. [44]. MGOAC (0.02 g) was added into 0.1 M KCl solution (20 mL). Then, the mixture was shaken for 10 min and kept for more than 24 h to establish equilibrium. The values of the initial and final solution pH were used to determine the pH_{pzc}.

4. Preparation of Dye Solution

Stock solution (1,000 mg/L AB113 dye) was prepared and stored in a dark place to avoid possible photodegradation of the dye. The stock solution was diluted to different concentrations by adding appropriate amount of deionized water. A calibration curve of AB113 dye was constructed from 10 mg/L to 100 mg/L with 10 mg/L interval to study the relationship between dye concentration and absorbance at maximum wavelength, λ_{max}, which in this case was 566 nm.

5. Adsorption Study

Response surface methodology (RSM) - Central composite design (CCD) was used to study the effect of operational parameters, including initial solution pH, adsorbent dosage and contact time on the adsorption of AB113 dye. The CCD approach was used to study the interaction between operational parameters with a fewer number of experiments [45-47]. Table 1 shows CCD with three

Table 1. Ranges of independent variables with their coded levels

Independent variables	Unit	Coded	Levels				
			$-\alpha$	Low (−1)	Medium (0)	High (+1)	$+\alpha$
pH	-	A	1.7	3	7	11	12.3
Adsorbent dosage	g/L	B	0.4	2	6	10	5.6
Time	h	C	1.4	2	4	6	6.6

adsorption parameters as independent variables.

The performance of the adsorbents in removing AB113 dye was evaluated through batch adsorption process. 100 mg/L of AB113 dye solution (20 mL) was put in an Erlenmeyer flask. To minimize the effect of ionic strength, 0.1 M H_2SO_4 and/or 0.1 M NaOH was used to adjust the solution pH to the required value [48]. A predetermined amount of adsorbents was added into the solution and the sample was covered by a cling film to avoid contamination. After that, the solution was shaken at 200 rpm using a rotary orbital shaker at 25 °C for a predetermined time. The color change was measured using a UV spectrophotometer (Spectro quant®, model Pharo 300) after filtering with a syringe filter (0.45 μm). The magnetic property of MGOAC facilitated the post-treatment separation of the composite from the solution with an external magnetic field. The efficiency of color removal and capacity of adsorption were calculated using Eq. (1) and Eq. (2).

$$\text{Colour removal (\%)} = \frac{\text{Colour}_{initial} - \text{Colour}_{final}}{\text{Colour}_{initial}} \times 100 \quad (1)$$

$$\text{Adsorption capacity (mg/g)} = \frac{(C_o - C_e)V}{W} \quad (2)$$

where C_o and C_e are AB113 dye concentration at initial and at equilibrium (mg/L), respectively; V is the sample solution volume (L), and W is the dosage of MGOAC (g).

6. Reusability Study

The adsorption-regeneration cycles were carried out five times to determine the stability and reusability of the MGOAC composite. 70% v/v ethanol was used as a green desorption agent to treat the used MGOAC. Deionized water was used to wash the treated MGOAC and it was then dried overnight at 60 °C before applying in the next cycle. The color removal efficiency and adsorption capacity for each cycle were recorded.

RESULTS AND DISCUSSION

1. Characterization

1-1. Textural Properties

BET and BJH analyses were used to study the textural properties of the MGOAC composite. The specific surface area, pore size and volume are provided in Table 2, while the nitrogen adsorption-desorption and the pore size distribution are shown in Fig. 1. The BET and Langmuir surface areas of 280.39 m^2/g and 309.97 m^2/g, respectively, indicate the composite has a high surface area. As can be seen from Fig. 1, MGOAC is a mesoporous composite that follows a type IV adsorption isotherm with a hysteresis loop. The surface area of the MGOAC composite is higher than other modified GO adsorbent reported by Sherlala et al. [43] (152.38 m^2/g), Liu et al. [49] (190.28 m^2/g), Abdi et al. [32] (226 m^2/g), Gao et al. [38] (53.83 m^2/g) and Hosseinzadeh and Ramin [36] (132.9 m^2/g).

Table 2. Summary of textural properties of MGOAC composite

Parameter	Unit	Value
BET surface area	m^2/g	280.39
Langmuir surface area	m^2/g	309.97
Average pore diameter	nm	4.99
Pore volume	cm^3/g	0.35

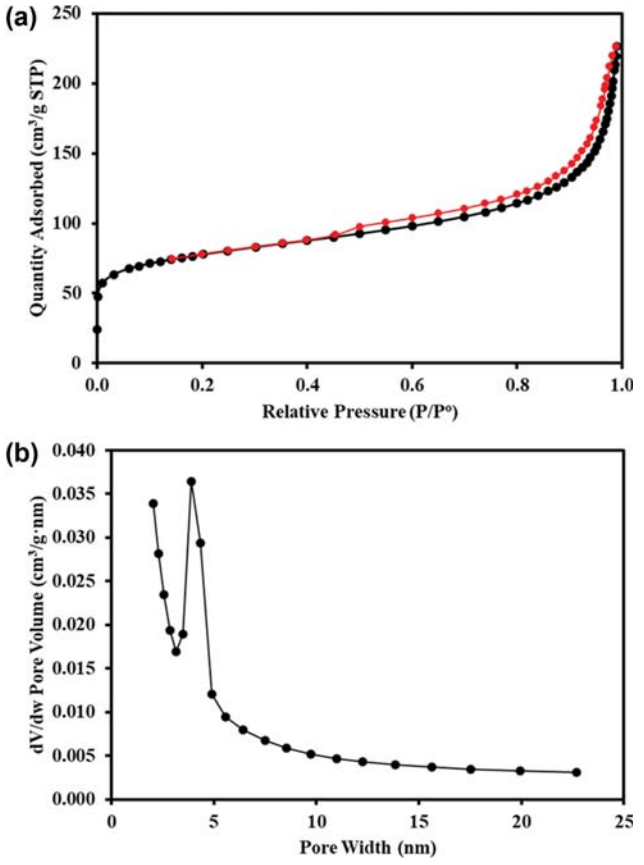

Fig. 1. (a) Nitrogen adsorption-desorption curve and (b) pore size distribution graph of MGOAC composite.

1-2. Morphology and Elemental Composition

The morphology and elemental composition of PKS-AC, GO and MGOAC composite were analyzed using SEM/EDX. Fig. 2(a) shows that the surface of PKS-AC is highly porous and offers a large surface area for adsorption process, while GO has a sheet-like struc-

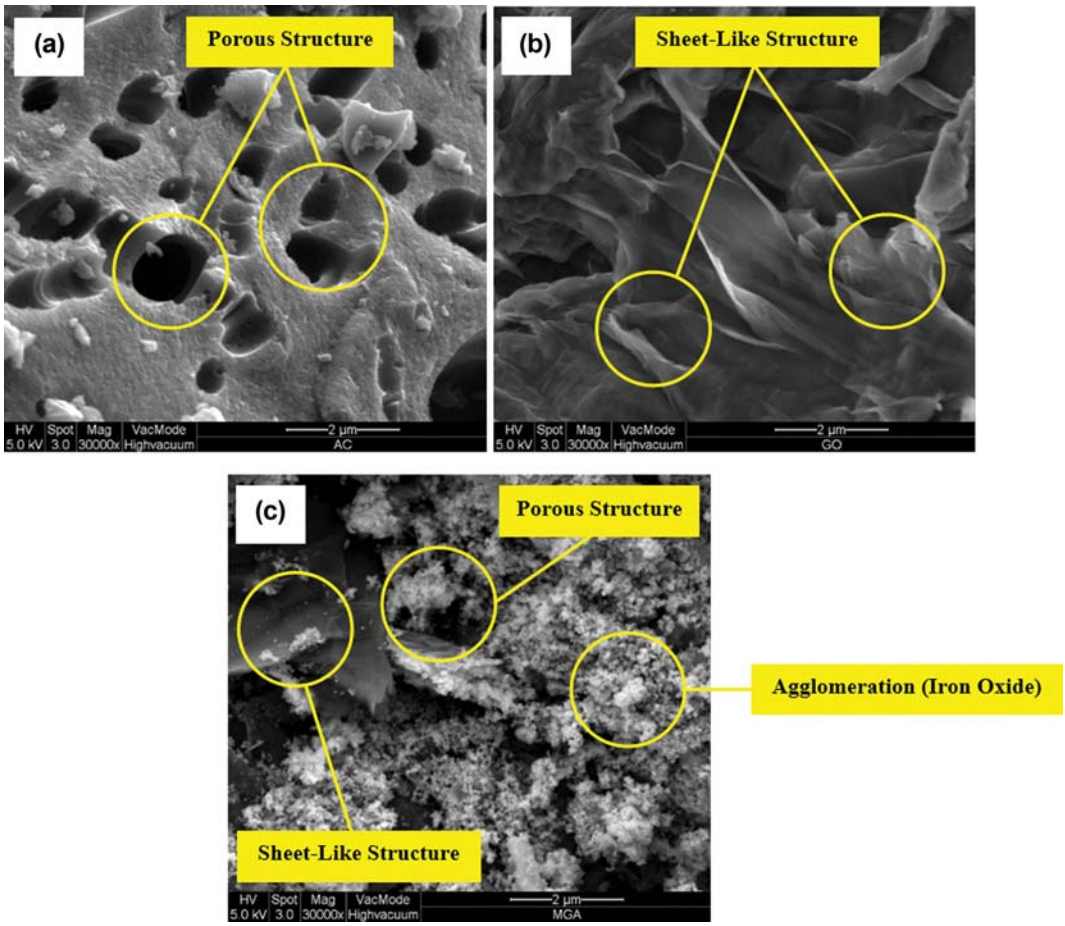

Fig. 2. SEM images of (a) PKS-AC (large pore size is observed), (b) GO (presence of sheet-like structure) and (c) MGOAC (agglomeration - iron oxide).

Table 3. EDX analysis of PKS-AC, GO and MGOAC

Material	Atomic (%)			
	Carbon (C)	Oxygen (O)	Sulphur (S)	Iron (Fe)
PKS-AC	93.99	6.01	-	-
GO	59.32	37.07	3.61	-
MGOAC	35.02	49.73	-	15.25

ture (Fig. 2(b)). The MGOAC composite in Fig. 2(c) shows both porous and sheet-like structure with an addition of agglomeration structure, which indicates the deposition of iron oxide.

Table 3 summarizes the chemical compositions of PKS-AC, GO and MGOAC. PKS-AC comprised of 93.99% carbon (C) atom and 6.01% of oxygen (O) atom. The GO has 59.32% C atom, with a higher amount of O (37.07%) and 3.61% of S atom. The presence of sulfur in GO may due to the contaminants in the graphite powder production. MGOAC composite comprised PKS-AC, GO and iron oxide. The presence of iron (Fe) atom (15.25%) and higher atomic percentage of oxygen (49.73%) indicated the successful deposition of iron oxide onto the surface of the composite. A reduction of C atom (35.02%) was observed for MGOAC, which was possibly due to the coverage of some C atoms by iron oxide.

1-3. Surface Functional Groups

Fig. 3 shows the FTIR spectra of MGOAC composite before and after the adsorption. The FTIR spectrum (Fig. 3(a)) shows that MGOAC composite exhibits peaks at 3,778 and 3,168 cm^{-1}, possibly originating from O-H stretching while O=C=O vibration is also observed with the peak at 2,331 cm^{-1}. The peaks observed at 1,877 cm^{-1} and 1,388 cm^{-1} are denoted by C-H bending. The peaks at 1,632, 1,575 and 970 cm^{-1} correspond to alkene group (C=C). The peaks at 1,263, 1,155 and 1,088 cm^{-1} represent C-O stretching. The presence of O-H, O=C=O, C-H, C=C and C-O groups is contributed by PKS-AC and GO. Furthermore, a peak at 540 cm^{-1} is due to the Fe-O bending, which is caused by the formation of iron oxide on the surface of MGOAC.

The intensity of the peak increased after adsorption compared to MGOAC composite before adsorption, as can be seen in Fig. 3(b). Some new peaks were observed in MGOAC composite after the adsorption process, which were possibly due to the formation of bonds between the dye and the adsorbent's functional groups [17]. The two new peaks observed at 1,657 and 2,009 cm^{-1} were caused by the vibration modes of imine (C=N) and isothiocyanate groups (N=C=S), respectively. The presence of imine and isothiocyanate groups proved that aniline ($C_6H_5NH_2$) and sodium

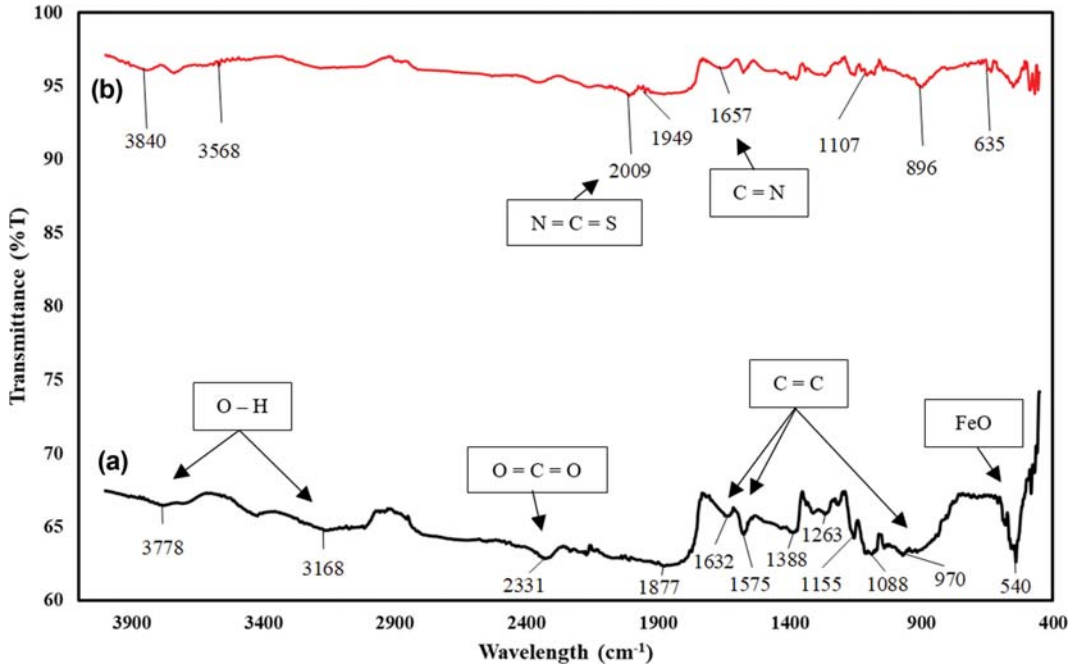

Fig. 3. FTIR spectra of MGOAC (a) before adsorption and (b) after adsorption.

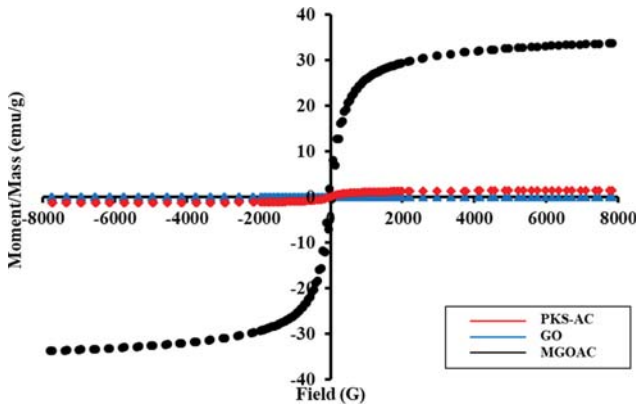

Fig. 4. VSM curve for PKS-AC, GO and MGOAC.

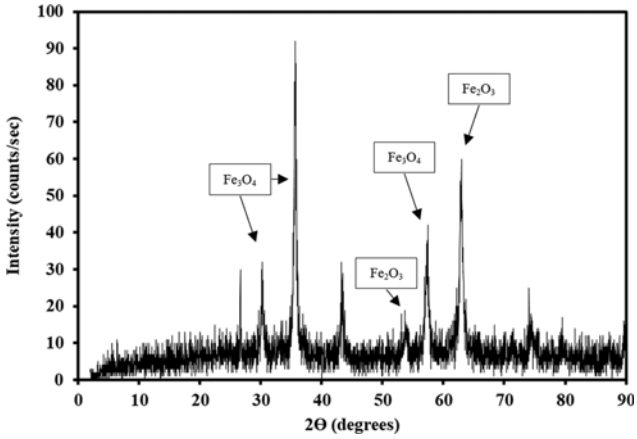

Fig. 5. XRD pattern of MGOAC.

benzenesulfonate ($C_6H_5NaSO_3$) groups from AB113 dye had formed bonds with the surface functional groups of the MGOAC composite. Details on the plausible adsorption mechanism of AB113 dye are discussed in subsection 8 (Results and Discussion).

1-4. Magnetic Properties

The magnetic property of the MGOAC composite was investigated using a vibrating sample magnetometer (VSM) and the result is presented in Fig. 4. There are three essential parameters in VSM analysis: saturation magnetization, coercivity and retentivity. Saturation magnetization represents the strength of the magnetic properties, while coercivity reveals the resistance of MGOAC to demagnetization. The capacity of MGOAC to stay magnetized even in the absence of a magnetic field is indicated by retentivity. In this case, 33.742 emu/g of magnetization indicates the composite has an excellent magnetic property, and is higher than some previous studies [32,36,38]. The coercivity of 45.094 G shows the excellent resistance of MGOAC to demagnetize, and 3.0817 emu/g retentivity indicates that the composite can maintain its magnetism in the absence of a magnetic field. The MGOAC composite shows a good magnetic property, which is essential for post-treatment separation by an external magnetic field. In contrast, magnetic property of PKS-AC and GO is negligible.

1-5. XRD

Fig. 5 shows the XRD pattern for MGOAC composite. The peaks observed at $2\theta \approx 27^{o}$ and 43^{o} can be related to carbon contributed by both PKS-AC and GO. On the other hand, peaks at 30^{o}, 36^{o} and 57^{o} indicate the presence of magnetite (Fe_3O_4) and maghemite (Fe_2O_3), while peaks at 54^{o} and 63^{o} show the existence of hematite (Fe_2O_3) that contributes to the magnetic properties of the composite [50]. The results confirmed that different forms of iron oxide have successfully deposited onto the surface of the composite.

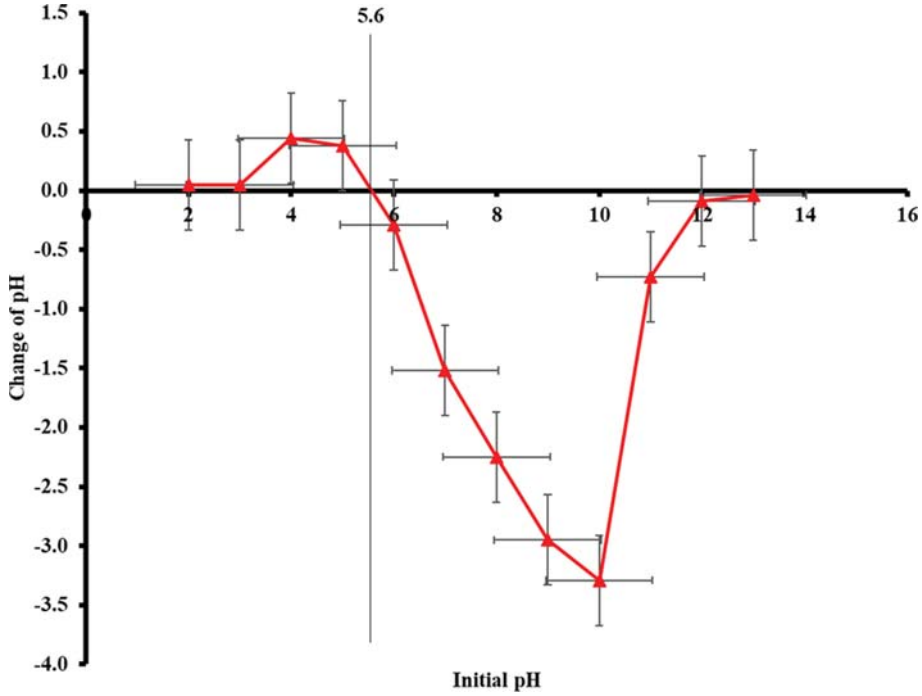

Fig. 6. pH_{pzc} plot of MGOAC.

Table 4. Response surface model equations for PKS-AC, GO and MGOAC on color removal and adsorption capacity in terms of actual factors

Response	Adsorbent	Response model
Color removal (%)	PKS-AC	$10.0-1.7A+15.0B+3.9C$
	GO	$-8.1+1.1A+35.2B+9.0C+1.5BC-4.8B^2-1.5C^2$
	MGOAC	$26.6+7.3A+33.3B+0.4C+0.6AB-1.1A^2-4.6B^2$
Adsorption capacity (mg/g)	PKS-AC	$87.8-7.1A-15.9B+0.7C+1.5AB$
	GO	$99.3-1.8A-27.9B-1.9C+0.4AB+0.7BC-2.0B^2$
	MGOAC	$105.7-1.9A-28.5B+0.2C+1.6AB-0.5A^2+1.5B^2$

1-6. pH_{pzc}

Fig. 6 shows a plot of pH_{pzc} for MGOAC composite. The pH_{pzc} is determined by the point that crosses the x-axis, which represents that there is no discrepancy between the initial and the final pH of the solution. This signifies the surface of MGOAC composite will have net surface charges above and below pH_{pzc}. The surface will be negatively charged above the pH_{pzc} and positively charged below pH_{pzc}. The pH_{pzc} of MGOAC is observed to be around 5.6. A similar study by Abdi et al. [32] also reported that the magnetic graphene oxide-modified composite has a pH_{pzc} of 5.4.

2. Adsorption Study

2-1. Response Surface Methodology and Statistical Analysis

RSM-CCD was used to show the effect of operational parameters on the color removal (%) and adsorption capacity (mg/g) and identify the optimal conditions. A total of 60 experiments were performed to analyze the adsorption properties of PKS-AC, GO and MGOAC. The effect of solution pH (pH 3-11), adsorbent dosage (1-5 g/L) and contact time (2-6 h) was studied to identify the optimal operational conditions.

The experimental run results based on RSM-CCD of color removal and adsorption capacity for PKS-AC, GO and MGOAC are presented in Supplementary (Table S1, S2 and S3). Based on the experimental results, model equations were developed to demonstrate the effect of the operational parameters on PKS-AC, GO and MGOAC performance. Table 4 depicts the models for PKS-AC, GO and MGOAC, where A, B and C represent solution pH, adsorbent dosage and contact time, respectively. The positive sign and negative sign in the equations indicate synergistic and antagonistic effects, respectively [51].

The experimental results for color removal and adsorption capacity of MGOAC composite were fitted into the reduced quadratic model. All the operational parameters have positive effects on the color removal, however, only the contact time shows a positive effect on adsorption capacity of MGOAC. On the other hand, the experimental results for color removal and adsorption capacity results using PKS-AC fitted well into the linear model and reduced 2FI model, respectively. Moreover, reduced quadratic models were established for both color removal and adsorption capacity using GO.

Analysis of variance (AVONA) was performed to investigate the suitability of the models. The ANOVA results are shown in Table

Table 5. ANOVA analysis for PKS-AC, GO and MGOAC

Response	Parameter	PKS-AC	GO	MGOAC
Color removal (%)	R^2	0.74	0.95	0.98
	Adjusted R^2	0.69	0.92	0.97
	Predicted R^2	0.57	0.85	0.93
	Mean square	3835.56	1836.53	2987.02
	F value	15.12	39.16	102.72
	Prob>F	<0.0001	<0.0001	<0.0001
	Adequate precision	12.46	19.71	28.97
Adsorption capacity (mg/g)	R^2	0.84	0.99	0.97
	Adjusted R^2	0.79	0.98	0.95
	Predicted R^2	0.69	0.95	0.88
	Mean square	894.95	919.76	1223.33
	F value	19.00	145.56	60.30
	Prob>F	<0.0001	<0.0001	<0.0001
	Adequate precision	13.95	38.97	28.02

5. For a model to be valid, four critical criteria need to be fulfilled. The adjusted R^2 must be in reasonable agreement with predicted R^2 and close to unity. Also, *prob>F* must be significant, i.e., less than 0.05. The adequate precision must be greater than four, and lack of fit must be insignificant, i.e., greater than 0.1. The *prob>F* value of <0.0001 was obtained for color removal and adsorption capacity in all cases, signifying that all the models were significant. Moreover, the adequate precision was more than 4 in all cases, which satisfies the requirement. Adequate precision of more than 4 implies that the models developed are suitable to be used for design space navigation.

In the case of color removal, the value of R^2 follows the sequences of MGOAC (0.98)>GO (0.95)>PKS-AC (0.74). The adjusted R^2 of MGOAC is 0.97 close to the predicted R^2 of 0.98. Besides, in the case of PKS-AC, the adjusted and predicted R^2 of 0.69 and 0.57, are close to each other but not close to 1, which indicates a large variation between the measured and predicted data. Moreover, the GO has an adjusted R^2 of 0.92, which is close to predicted R^2 of 0.85 for color removal. Predicted R^2 of 0.93, 0.57 and 0.85 indicate that 93%, 57% and 85% of the color removal using MGOAC, PKS-AC and GO, respectively, can be explained by the model developed by RSM-CCD. In the case of adsorption capacity, the R^2 value (0.97) of MGOAC is slightly lower than GO (0.99) but still close to unity.

3. Comparison of PKS-AC, GO and MGOAC

Fig. 7 represents the comparison between PKS-AC, GO and MGOAC. As can be seen, MGOAC achieved the highest color removal and adsorption capacity under acidic (pH 3: 96.9%, 19.4 mg/g) and neutral conditions (pH 7: 96.3%, 32.2 mg/g) compared to PKS-AC and GO. However, under basic condition (pH 11), both PKS-AC and GO achieved higher performance than MGOAC. MGOAC achieved the highest adsorption capacity (32.2 mg/g) among the three types of adsorbents at neutral condition, as shown in Fig. 7(b). The MGOAC was found to achieve higher performance compared to virgin materials alone, which could be explained by the combination of various functional groups from PKS-AC, GO and iron oxide that aid in the bond formation between adsorbent and adsorbate [52]. The result is further supported by some previous works [52-54].

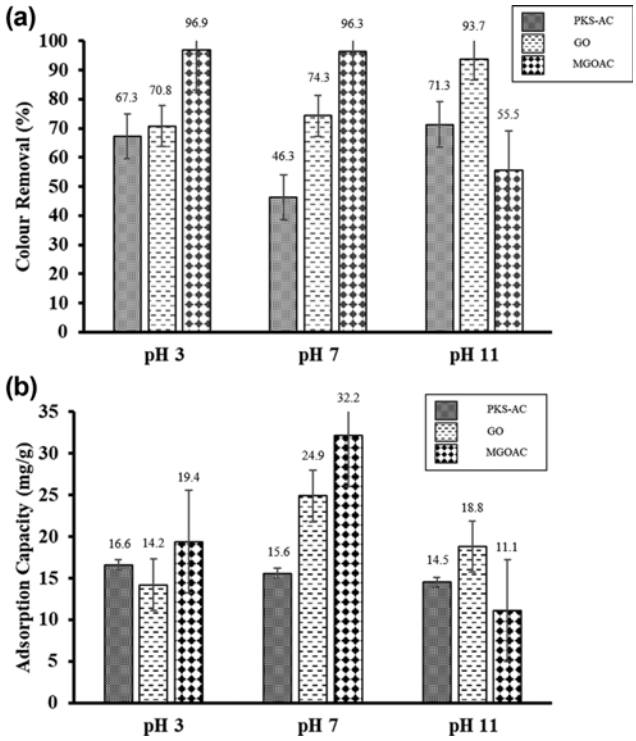

Fig. 7. Comparison of (a) color removal and (b) adsorption capacity of PKS-AC, GO and MGOAC at different pH.

The performance of the MGOAC under acidic conditions could be explained by considering the pH_{pzc} of the adsorbent and the ionic state of the pollutant. The pH_{pzc} of the MGOAC is 5.6 while AB113 is anionic. Thus, at pH 3, the surface of the MGOAC is positive, leading to the attraction of the anionic dye. However, under the neutral condition, complexation may occur between the surface functional groups and the dye. On the other hand, under pH 11, surface of the MGOAC is negatively charged, repelling the

anionic dye from the surface. This implies that the adsorption process could be controlled by both electrostatic interaction and surface complexation.

4. Effect of Operational Parameters

The effects of initial pH of the solution (A), adsorbent dosage (B) and contact time of adsorption (C) were studied to identify the optimal conditions for maximum color removal and adsorption capacity. Since RSM could be used to understand the interactions of different operational parameters, 2-dimensional plots are presented to visualize such interactions.

4-1. Effect of Initial Solution pH

The initial pH of the solution is important in adsorption process, as the adsorbent surface charge may be changed (protonated or deprotonated) with the presence of protons in the solution [55,56]. In this study, the effect of pH, in the range of 3 to 11 was investigated. Fig. 8 shows the 2D plots of interaction between operational parameters for color removal. As can be seen from Fig. 8(a), the color removal decreased from 70.7% to 10.5% when solution pH was increased from 3 to 11 at a contact time of 4 h using 1 g/L of MGOAC. However, when the MGOAC dosage varied from 1 to 2.4 g/L, the color removal efficiency increased from 49.8% to 80.8% even at slightly alkaline condition (around pH 8). This finding is similar to that reported by Li et al. [14].

The effect of solution pH can also be explained by considering the pH_{pzc} of MGOAC composite. The pH_{pzc} of the MGOAC was 5.6, indicating that its surface was positively charged below pH 5.6

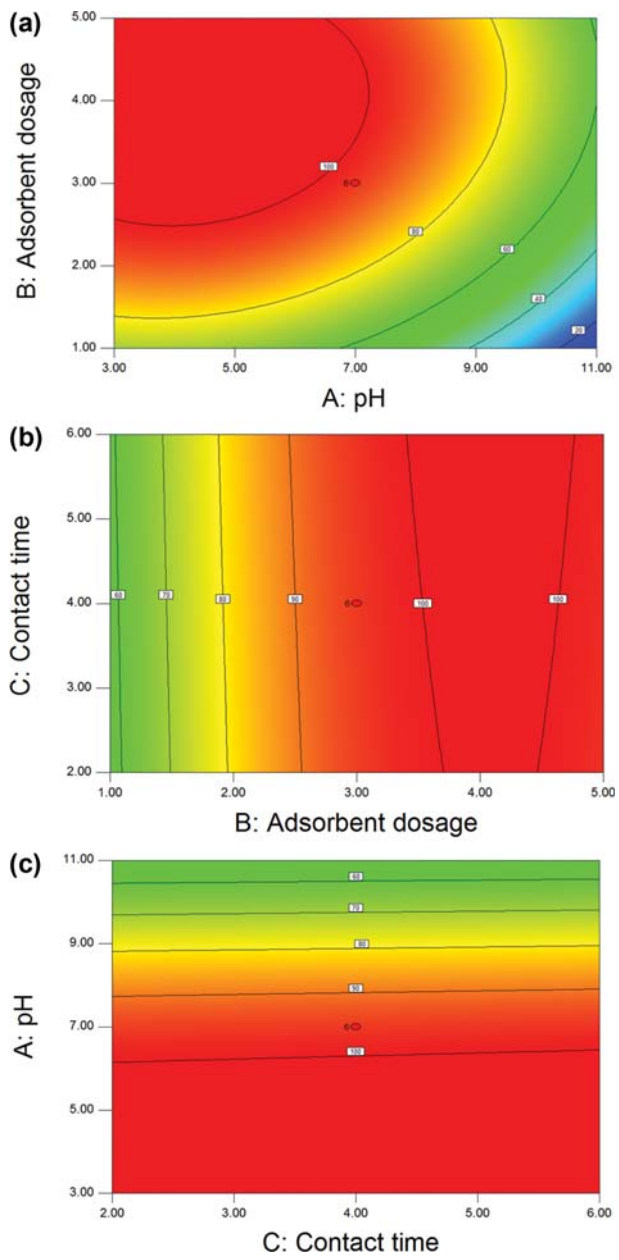

Fig. 8. Effect of operating parameters on the removal efficiency of AB113 by MGOAC.

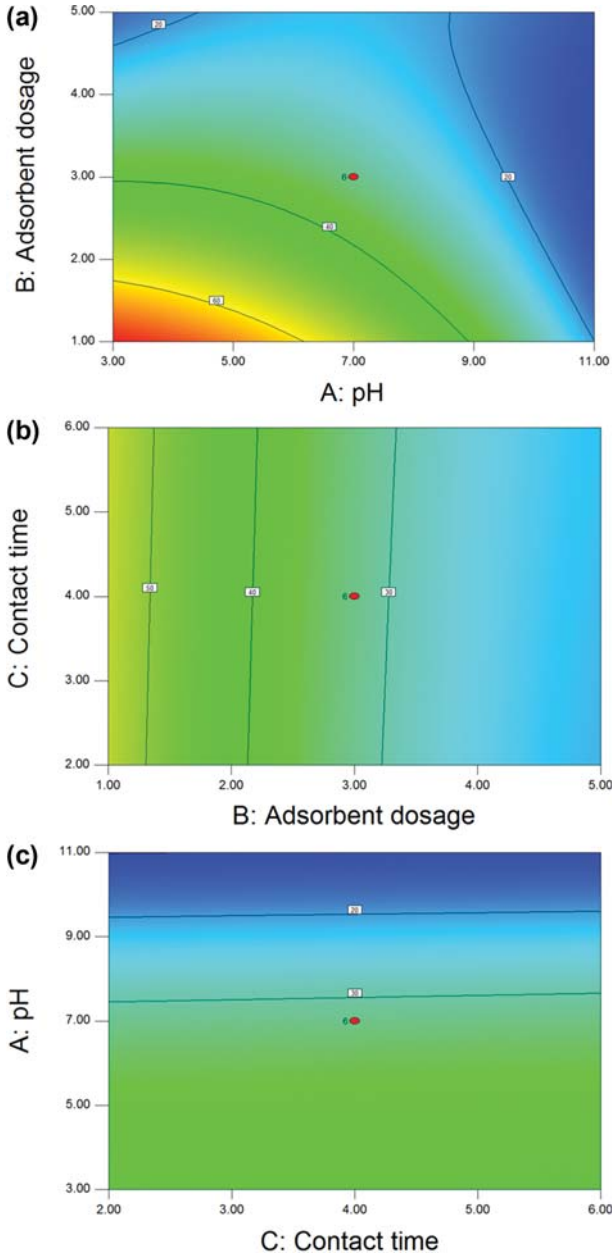

Fig. 9. Effect of operating parameters on the adsorption capacity of MGOAC for the removal of AB113.

and negatively charged above this value. Since AB113 is an anionic dye, there will be electrostatic attraction below the pH_{pzc} while electrostatic repulsion is expected above the pH_{pzc}. Thus, high removal was achieved under acidic conditions. However, as observed from the results, higher adsorptive removals could also be achieved under alkaline condition, which indicates that other mechanisms, such as surface complexation, are possible.

Fig. 9(a) shows the interaction between initial solution pH and MGOAC dosage on the adsorption capacity. As depicted in Fig. 9(a), MGOAC achieved the highest adsorption capacity under the acidic condition. The adsorption capacity decreased when the solution pH increased from 3 to 11. This is because AB113 dye is an anionic dye and its adsorption is favored when solution pH< pH_{pzc} (5.6) [57]. Similar findings were reported by Jain et al. [2].

4-2. Effect of Adsorbent Dosage

The effect of MGOAC dosage on the color removal was investigated by varying the dosage from 1 to 5 g/L. Color removal was found to be increased from 58.6 to 97.6% when the amount of MGOAC was varied from 1 to 5 g/L at neutral conditions and 4 h contact time (Fig. 8(a)). This may be possible because of the increase in the number of active sites available for the adsorption with the adsorbent dosage [58]. As can be seen in Fig. 8(a), complete color removal is achieved using only 2.6 g/L of MGOAC at pH 3. However, at neutral pH, the same system required 3.5 g/L of MGOAC to achieve complete color removal. The increasing of adsorbent dosage above 3.5 g/L only has a little contribution to the color uptake, possibly because the system has reached adsorption equilibrium. In conclusion, highest color removal efficiency is achieved between pH 3 to pH 7.3 by varying amount of MGOAC (ranges from 2.5 to 5 g/L) at 4 hours of contact time.

Fig. 9(b) shows the effect of MGOAC dosage and contact time on the adsorption capacity. The adsorption capacity decreased from 74.2 to 16.4 mg/g when the MGOAC dosage was increased from 1 to 5 g/L at pH 3 and 4 h contact time. Based on Eq. (2), the denominator is the adsorbent dosage which has a dominant effect on the capacity of adsorption. The decrease in adsorption capacity at higher adsorbent dosage can be explained by the aggregation of the composite, which could reduce the effective active sites and surface area of the composite [59]. Hence, when adsorbent dosage increased, the adsorption capacity of MGOAC composite decreased and vice versa.

4-3. Effect of Contact Time

The contact time of the adsorption process was varied from 2 to 6 h to study its effect on the AB113 adsorption. The effect of contact time was found to be insignificant compared to the effect of initial solution pH and adsorbent dosage, as shown in Fig. 8(b) and 8(c) for color removal and Fig. 9(b) and 9(c) for adsorption capacity. Color removal only increased from 57.5% to 58.9% (1.4%) when the contact time was increased from 2 to 6 h (Fig. 8(b)) at pH 7 using 1 g/L of MGOAC. On the other hand, as depicted in Fig. 9(c), when the solution was at pH 3, there was only slight increase in adsorption capacity from 38.8 to 39.7 mg/g (0.9 mg/g) when the contact time increased from 2 to 6 h. This is because most of the adsorption of AB113 dye on MGOAC occurred in the first two hours of the adsorption process. This phenomenon can be explained by abundant active sites present at the beginning of the adsorption process. However, as the adsorption proceeds, most of the active sites will be occupied by the dye, decreasing the dye uptake with increase in contact time [60]. Hence, the contact time does not significantly affect the color removal and adsorption capacity within the range of investigation.

5. Adsorption Kinetics

Adsorption kinetics was studied to determine the rate of the AB113 adsorbed as well as its mechanism [7]. To study the kinetics model for the adsorption of AB113 dye onto MGOAC, three most commonly used models, pseudo-first-order (P-F-O), pseudo-second-order (P-S-O) and intra-particle (I-P) models, were used. Eqs. (3) to (5) represent the P-F-O, P-S-O and I-P models, respectively.

$$\log(q_e - q_t) = -\frac{k_1}{2.303}t + \log q_e \tag{3}$$

$$\frac{t}{q_t} = \frac{1}{q_e}t + \frac{1}{k_2 q_e^2} \tag{4}$$

$$q_t = k_i t^{1/2} + c \tag{5}$$

where the quantity of AB113 dye adsorbed per weight of MGOAC at equilibrium and at time t (mg g^{-1}) is denoted as q_e and q_t, respectively. Besides, rate constants for P-F-O and P-S-O models are denoted as k_1 (min^{-1}) and k_2 (g mg^{-1} min^{-1}), respectively, while intra-particle diffusion rate coefficient is denoted as k_i (mg g^{-1} $min^{-0.5}$). c represents the thickness of the boundary layer constant.

The outcomes of kinetic parameters are summarized in Table 6, while the graphs of three different models are provided in Supplementary (Fig. S1) material. The adsorption of AB113 dye onto MGOAC can be best demonstrated by the P-S-O model based on the coefficient determination (R^2 value), with P-S-O model having the highest R^2 value (1.00). On the other hand, I-P model also reported almost similar R^2 value (0.98). Therefore, the adsorption of AB113 dye onto MGOAC is possibly controlled by both chemisorption and pore diffusion. The result is consistent with the previous research on the adsorption of different types of synthetic dye using modified graphene oxide composites [32,38,61].

Additionally, Fig. 10 shows the adsorption rate curve of MGOAC over 2.1 h. Most of the adsorption occurs in the first 10 min, as shown in both Fig. 10(a) and 10(b). This is because more active sites are present at the beginning of the process for adsorption to occur [62]. As time goes on, the active sites decrease due to the rapid uptake of the AB113 in the beginning of time.

6. Adsorption Isotherm

The isotherm parameters and underlying thermodynamic as-

Table 6. Kinetic parameters of AB113 dye adsorption onto MGOAC composite

Kinetic model	Parameter	Unit	Value	R^2
P-F-O	k_1	min^{-1}	0.05	0.79
	q_e	mg g^{-1}	15.41	
P-S-O	k_2	g mg^{-1} min^{-1}	0.01	1.00
	q_e	mg g^{-1}	27.86	
I-P	k_i	mg g^{-1} $min^{-0.5}$	0.62	0.98
	c	-	20.29	

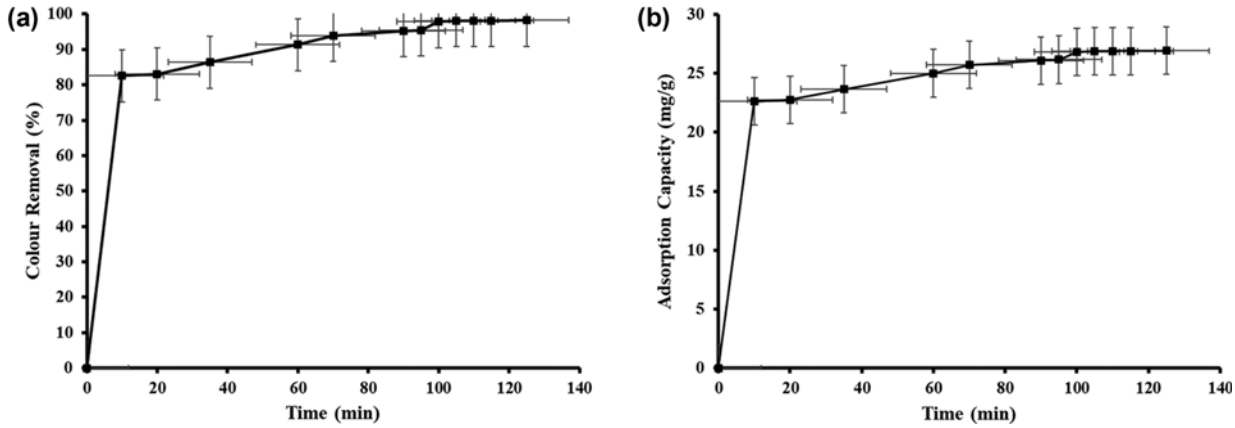

Fig. 10. Adsorption rate curves for (a) color removal efficiency and (b) adsorption capacity at optimal condition (pH 7.5, 3.7 g/L MGOAC, 2.1 h).

sumptions usually give essential information regarding an adsorbent's mechanism, surface properties and affinity [63]. Three well-known isotherms, Langmuir, Freundlich and Temkin, were used to study the behavior of AB113 dye adsorbed onto MGOAC composite. Eqs. (6) to (8) represent the Langmuir, Freundlich and Temkin isotherms, respectively.

$$\frac{C_e}{q_e}=\left[\frac{1}{Q^o}\right]C_e+\left[\frac{1}{Q^o b}\right] \quad (6)$$

$$\log q_e=\frac{1}{n}\log C_e+\log k_f \quad (7)$$

$$q_e=B_1\ln C_e+B_1\ln A_1 \quad (8)$$

where Q^o is the amount of AB113 dye adsorbed per weight of MGOAC at monolayer (mg/g), b (L/mg) and k_f ($mg^{1-n}\,L^n\,g^{-1}$) are Langmuir constant and Freundlich constant, respectively while B_1 (no unit) and A_1 (L/g) are constants for heat of sorption and equilibrium binding, respectively.

The equilibrium parameters for adsorption of AB113 dye onto MGOAC are shown in Table 7. The graphs for three different isotherm models are shown in Supplementary (Fig. S2). The separation factor, R_L, is a crucial parameter in the Langmuir isotherm model which reveals the favorability of the adsorption process. Eq. (9) was used to obtain R_L value.

$$R_L=\frac{1}{1+bC_o} \quad (9)$$

Table 7. Adsorption isotherm parameters of AB113 dye adsorption onto MGOAC

Isotherm model	Parameter	Unit	Value	R^2
Langmuir	Q^o	$mg\,g^{-1}$	86.96	1.00
	b	$L\,mg^{-1}$	0.19	
	R_L	-	0.01	
Freundlich	k_f	$mg^{1-n}\,L^n\,g^{-1}$	49.65	0.99
	n	-	9.52	
Tempkin	A_1	$L\,g^{-1}$	681.59	0.99
	B_1	-	7.24	

In this case, an R_L value of 0.01 which is $0<R_L<1$ indicates the adsorption process is desirable [32,64].

Among the three isotherm models, Langmuir has the highest R^2 value of 1.00, which indicates the adsorption of AB113 dye on MGOAC is monolayer adsorption. Since adsorption of AB113 on MGOAC fitted well into Langmuir and P-S-O models, the adsorption process can be considered as monolayer chemisorption process.

The maximum monolayer adsorption capacity of 86.96 mg/g is higher than other adsorbents in removing AB113 dye, such as 59.81 mg/g as reported by Lee et al. [56] using overripe Cucumis sativus peel and 83.30 mg/g reported by Shirzad-Siboni et al. [65] using activated red mud. The adsorption capacity is also comparable to the results reported by Bach et al. [44] (42.2-80.6 mg/g) for the removal of Methylene Blue using graphene oxide-doped with different metals (Co, Mn and Ni). On the other hand, the adsorption capacity is lower than the 147 mg/g reported by Abd-Elhamid et al. [6] for the removal of Methylene Blue using graphene oxide-activated carbon (GO-AC) composite.

7. Regeneration and Reusability

The reusability study explains the adsorbent's stability and ability to be regenerated after adsorption [66]. The reusability study

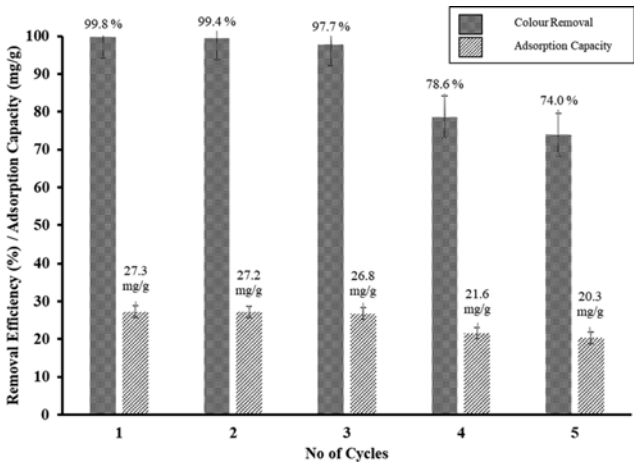

Fig. 11. Reusability of MGOAC over five cycles (pH 7.5, 3.7 g/L MGOAC, 2.1 h).

was carried out at optimal conditions (pH 7.5 and 2.1 h using 3.7 g/L of MGOAC). 70% v/v ethanol (C_2H_5OH) was utilized as a green desorption agent in regenerating the used adsorbent [67]. Fig. 11 shows that the color removal efficiency decreased from 99.8% in the first cycle to 74.0% in the fifth cycle. The gradual reduction in color removal efficiency was due to the dye not being fully desorbed from the surface of the MGOAC [68]. However, the MGOAC still achieved more than 70% of color removal after the fifth cycle, signifying the excellent reusability and stability of the MGOAC. The reusability of MGOAC is higher than surfactant modified fallen leaves adsorbent using same dye solution (AB113 dye) [60]. A reduction of 2.1% of color removal was recorded for MGOAC at third cycle, which is six-times lower compared to 12.1% of color removal reduction of surfactant modified fallen leaves. The ability of MGOAC to be reused for several cycles is a merit for operational cost reduction in industrial applications.

8. Plausible Adsorption Mechanism

A plausible mechanism for AB113 dye adsorption onto MGOAC composite is proposed considering initial solution pH, pH_{pzc} as well as FTIR analysis. In this study, the pH_{pzc} of the MGOAC was found to be 5.6. On the other hand, the color of AB113 dye is contributed by complex functional groups, including sodium benzenesulfonate ($C_6H_5NaSO_3$) and aniline ($C_6H_5NH_2$) groups. From the results, high color removal was obtained both at acidic and neutral conditions. This indicates that the adsorption of AB113 dye onto MGOAC could be both through electrostatic interaction and surface complex formation between the functional group of AB113 dye and surface of MGOAC composite. Eqs. (10) and (11) propose a possible bond formation mechanism between $C_6H_5NaSO_3$ and $C_6H_5NH_2$ with functional group found on the surface of MGOAC composite. This proposed mechanism is in good agreement with similar work reported by previous researchers [69,70], where the adsorption mechanism could be through the two different processes. A two-dimensional graphical presentation of the plausible adsorption mechanism is presented in Supplementary (Fig. S3).

$$C{=}C+2C_6H_5NH_2 \rightarrow 2C_6H_5N{=}C+2H_2 \quad (10)$$

$$C_6H_5N{=}C+C_6H_5NaSO_3 \rightarrow C_6H_5N{=}C{=}SO_3+C_6H_5Na+H_2 \quad (11)$$

CONCLUSION

MGOAC composite was successfully synthesized and used to remove AB113 dye from aqueous solution. The MGOAC composite possesses mesoporous properties with a specific surface area of 280.39 m^2/g and a saturation magnetization of 33.72 emu/g. The developed composite exhibited higher performance than either PKS-AC or GO. The composite exhibited an adsorption capacity of 27.3 mg/g, removing up to 99.8% of color under optimal conditions. The adsorption of AB113 dye onto MGOAC shows maximum monolayer adsorption capacity of 86.96 mg/g. Besides, the MGOAC composite was able to maintain dye removal efficiency up to 74.0% over five adsorption-desorption cycles. The presence of iron oxide facilitates the post-treatment separation using an external magnet. This study has shown that the newly developed MGOAC composite has the potential to be used as an adsorbent for the removal of textile dyes from wastewater. It is envisaged that the adsorbent developed in this study could be applicable for the removal of different organic pollutants found in wastewater. The incorporation of agricultural waste-based activated carbon will be useful for industrial applications, where treatment cost becomes a significant factor.

ACKNOWLEDGEMENT

This work was supported by the Fundamental Research Grant Scheme (FRGS) provided by Ministry of Education (MOE), Malaysia with grant number FP141-2019A.

ABBREVIATIONS

Symbols

A_1 : constant for equilibrium binding [L/g]
AB113 : Acid Blue 113 [-]
ANOVA : analysis of variance [-]
b : Langmuir constant [L/mg]
B_1 : constant for heat of sorption [-]
BET : Brunauer-Emmett-Teller [-]
BJH : Barrett-Joyner-Halenda [-]
C : carbon [-]
c : thickness of the boundary layer constant [-]
C=C : alkene [-]
C=N : imine [-]
C_2H_5OH : ethanol [-]
$C_6H_5NaSO_3$: sodium benzenesulfonate [-]
$C_6H_5NH_2$: aniline [-]
CCD : central composite design [-]
C_e : AB113 dye concentration at equilibrium [mg/L]
CH_3COOH : acetic acid [-]
C_o : AB113 dye concentration at initial [mg/L]
Fe : iron [-]
Fe_2O_3 : Hematite; Maghemite; [-]
Fe_3O_4 : magnetite [-]
$FeCl_2{\cdot}4H_2O$: ferrous chloride tetrahydrate [-]
$FeCl_3{\cdot}6H_2O$: iron (III) chloride hexahydrate [-]
FTIR : fourier transformation infrared [-]
GO : graphene oxide [-]
H_2O_2 : hydrogen peroxide [-]
H_2SO_4 : sulphuric acid [-]
HCl : hydrochloric acid [-]
I-P : intra-particle [-]
k_1 : rate constant for P-F-O [min^{-1}]
k_2 : rate constant for P-S-O [g mg^{-1} min^{-1}]
KCl : potassium chloride [-]
k_f : Freundlich constant [mg^{1-n} L^n g^{-1}]
k_i : intraparticle diffusion rate coefficient [mg g^{-1} $min^{-0.5}$]
$KMnO_4$: potassium permanganate [-]
MGOAC : magnetic graphene oxide-activated carbon [-]
N=C=S : isothiocyanate [-]
NaOH : sodium hydroxide [-]
NH_4OH : ammonium hydroxide [-]
O : oxygen [-]

P-F-O: pseudo-first-order [-]
pH_{pzc} : point of zero charge [-]
PKS-AC : palm kernel shell-based activated carbon [-]
P-S-O: pseudo-second-order [-]
q_e : quantity of AB113 dye adsorbed per weight of MGOAC at equilibrium [mg/g]
Q^o : amount of AB113 dye adsorbed per weight of MGOAC at monolayer [mg/g]
q_t : quantity of AB113 dye adsorbed per weight of MGOAC at time t [mg/g]
R^2 : coefficient of determination [-]
R_L : separation factor [-]
rpm : revolutions per minute [-]
RSM : response surface methodology [-]
S : sulfur [-]
SEM/EDX : scanning electron microscopy coupled with energy dispersive X-ray [-]
t : time [min]
V : sample solution volume [L]
VSM : vibrating-sample magnetometer [-]
W : dosage of MGOAC [g]
XRD : X-ray diffraction [-]

SUPPORTING INFORMATION

Additional information as noted in the text. This information is available via the Internet at http://www.springer.com/chemistry/journal/11814.

REFERENCES

1. J. Martín, M. D. M. Orta, S. Medina-Carrasco, J. L. Santos, I. Aparicio and E. Alonso, *Environ. Res.*, **164**, 488 (2018).
2. S. N. Jain, S. R. Tamboli, D. S. Sutar, S. R. Jadhav, J. V. Marathe, A. A. Shaikh and A. A. Prajapati, *J. Clean. Prod.*, **252**, 119778 (2020).
3. P. Mehdizadeh, Y. Orooji, O. Amiri, M. Salavati-Niasari and H. Moayedi, *J. Clean. Prod.*, **252**, 119765 (2020).
4. Y. W. Kim, J. H. Kim, D. H. Moon and H. J. Shin, *Korean J. Chem. Eng.*, **36**, 101 (2019).
5. A. Pirkarami and M. E. Olya, *J. Saudi Chem. Soc.*, **21**, S179 (2017).
6. A. I. Abd-Elhamid, E. A. Kamoun, A. A. El-Shanshory, H. M. A. Soliman and H. F. Aly, *J. Mol. Liq.*, **279**, 530 (2019).
7. A. M. Aljeboree, A. N. Alshirifi and A. F. Alkaim, *Arab. J. Chem.*, **10**, S3381 (2017).
8. S. Tian, S. Xu, J. Liu, C. He, Y. Xiong and P. Feng, *J. Clean. Prod.*, **239**, 117767 (2019).
9. A. L. D. Rosa, E. Carissimi, G. L. Dotto, H. Sander and L. A. Feris, *J. Clean. Prod.*, **198**, 1302 (2018).
10. M. Naushad, A. A. Alqadami, Z. A. AlOthman, I. H. Alsohaimi, M. S. Algamdi and A. M. Aldawsari, *J. Mol. Liq.*, **293**, 111442 (2019).
11. C. H. Nguyen and R.-S. Juang, *J. Taiwan Inst. Chem. Eng.*, **99**, 166 (2019).
12. N. P. Khumalo, G. D. Vilakati, S. D. Mhlanga, A. T. Kuvarega, B. B. Mamba, J. Li and D. S. Dlamini, *J. Water Process Eng.*, **31**, 100878 (2019).
13. G. Kyriakopoulos, I. Xiarchos and D. Doulia, *Int. J. Environ. Technol. Manag.*, **6**, 515 (2006).
14. Y. Li, Q. Du, T. Liu, X. Peng, J. Wang, J. Sun, Y. Wang, S. Wu, Z. Wang, Y. Xia and L. Xia, *Chem. Eng. Res. Des.*, **91**, 361 (2013).
15. R. Sahraei, Z. S. Pour and M. Ghaemy, *J. Clean. Prod.*, **142**, 2973 (2017).
16. P. Ranjan, J. Balakrishnan and A. D. Thakur, *Mater. Today Proc.*, **11**, 833 (2019).
17. P. Pal and A. Pal, *J. Water Process Eng.*, **31**, 100882 (2019).
18. G. Kyriakopoulos and D. Doulia, *Fresenius Environ. Bull.*, **16**, 731 (2007).
19. J. Roh, H. N. Umh, C. M. Yoo, S. Rengaraj, B. Lee and Y. Kim, *Korean J. Chem. Eng.*, **29**, 903 (2012).
20. J. Pérez-Calderón, M. V. Santos and N. Zaritzky, *J. Environ. Chem. Eng.*, **6**, 6749 (2018).
21. W. Xiao, Z. N. Garba, S. Sun, I. Lawan, L. Wang, M. Lin and Z. Yuan, *J. Clean. Prod.*, **253**, 119989 (2020).
22. S. Wong, H. H. Tumari, N. Ngadi, N. B. Mohamed, O. Hassan, R. Mat and N. A. S. Amin, *J. Clean. Prod.*, **206**, 394 (2019).
23. A. A. Peláez-Cid, V. Romero-Hernández, A. M. Herrera-González, A. Bautista-Hernández and O. Coreño-Alonso, *Chinese J. Chem. Eng.*, **28**, 613 (2019).
24. L. P. Lingamdinne, J.-S. Choi, Y.-L. Choi, J.-K. Yang, J. R. Koduru and Y. Chang, *Metals (Basel).*, **9**, 1 (2019).
25. N. Singh, S. Riyajuddin, K. Ghosh, S. Mehta and A. Dan, *ACS Appl. Nano Mater.*, **2**, 7379 (2019).
26. Y. Orooji, F. Liang, A. Razmjou, G. Liu and W. Jin, *Sep. Purif. Technol.*, **205**, 273 (2018).
27. F. Tahmasebi, M. Alimohammadi, R. Nabizadeh, M. Khoobi, K. Karimian and A. Zarei, *Korean J. Chem. Eng.*, **36**, 894 (2019).
28. L. P. Lingamdinne, J. R. Koduru and R. R. Karri, *J. Environ. Manage.*, **231**, 622 (2019).
29. R. Nasiri and N. Arsalani, *J. Clean. Prod.*, **190**, 63 (2018).
30. Y. Jiang, J. L. Gong, G. M. Zeng, X. M. Ou, Y. N. Chang, C. H. Deng, J. Zhang, H. Y. Liu and S. Y. Huang, *Int. J. Biol. Macromol.*, **82**, 702 (2016).
31. Y. Zhang, H. Li, M. Li and M. Xin, *J. Mol. Struct.*, **1209**, 127973 (2020).
32. G. Abdi, A. Alizadeh, J. Amirian, S. Rezaei and G. Sharma, *J. Mol. Liq.*, **289**, 111118 (2019).
33. H. Karimi-Maleh, M. Shafieizadeh, M. A. Taher, F. Opoku, E. M. Kiarii, P. P. Govender, S. Ranjbari, M. Rezapour and Y. Orooji, *J. Mol. Liq.*, **298**, 112040 (2020).
34. I. Ali, A. Arsh, X. Y. Mbianda, A. Burakov, E. Galunin, I. Burakova, E. Mkrtchyan, A. Tkachev and V. Grachev, *Environ. Int.*, **127**, 160 (2019).
35. G. Yao, W. Bi and H. Liu, *Colloids Surf. A Physicochem. Eng. Asp.*, **588**, 124393 (2020).
36. H. Hosseinzadeh and S. Ramin, *Int. J. Biol. Macromol.*, **113**, 859 (2018).
37. J.-Y. Chen, S.-R. Cao, C.-X. Xi, Y. Chen, X.-L. Li, L. Zhang, G.-M. Wang, Y.-L. Chen and Z.-Q. Chen, *Food Chem.*, **239**, 911 (2018).
38. M. Gao, Z. Wang, C. Yang, J. Ning, Z. Zhou and G. Li, *Colloids Surf. A Physicochem. Eng. Asp.*, **566**, 48 (2019).
39. S. Mishra, S. S. Yadav, S. Rawat, J. Singh and J. R. Koduru, *J. Environ. Manage.*, **246**, 362 (2019).
40. G. Asgari, A. Shabanloo, M. Salari and F. Eslami, *Environ. Res.*,

184, 109367 (2020).
41. Y. Orooji, M. Ghanbari, O. Amiri and M. Salavati-Niasari, *J. Hazard. Mater.*, **389**, 122079 (2020).
42. F. A. Taher, F. H. Kamal, N. A. Badawy and A. E. Shrshr, *Mater. Res. Bull.*, **97**, 361 (2018).
43. A. I. A. Sherlala, A. A. A. Raman, M. M. Bello and A. Buthiyappan, *J. Environ. Manage.*, **246**, 547 (2019).
44. L. G. Bach, T. V. Tran, T. D. Nguyen, T. V. Pham and S. T. Do, *Res. Chem. Intermed.*, **44**, 1661 (2018).
45. L. P. Lingamdinne, K. R. Vemula, Y. Y. Chang, J. K. Yang, R. R. Karri and J. R. Koduru, *Chemosphere*, **243**, 125257 (2020).
46. M. O. Saeed, K. Azizli, M. H. Isa and M. J. K. Bashir, *J. Water Process Eng.*, **8**, e7 (2015).
47. Ş. Yılmaz, T. Şahan and A. Karabakan, *Korean J. Chem. Eng.*, **34**, 2225 (2017).
48. G. Kyriakopoulos, D. Doulia and A. Hourdakis, *Int. J. Environ. Anal. Chem.*, **86**, 207 (2006).
49. S. Liu, M. Li, Y. Liu, N. Liu, X. Tan, L. Jiang, J. Wen, X. Hu and Z. Yin, *J. Taiwan Inst. Chem. Eng.*, **102**, 330 (2019).
50. F. Iranpour, H. Pourzamani, N. Mengelizadeh, P. Bahrami and H. Mohammadi, *J. Environ. Chem. Eng.*, **6**, 3418 (2018).
51. S. K. Behera, H. Meena, S. Chakraborty and B. C. Meikap, *Int. J. Min. Sci. Technol.*, **28**, 621 (2018).
52. A. Muhammad, A. H. A. Shah and S. Bilal, *Appl. Sci.*, **10**, 2882 (2020).
53. L. Li, X. L. Liu, H. Y. Geng, B. Hu, G. W. Song and Z. S. Xu, *J. Mater. Chem. A*, **1**, 10292 (2013).
54. N. Wahab, M. Saeed, M. Ibrahim, A. Munir, M. Saleem, M. Zahra and A. Waseem, *Front. Chem.*, **7**, 1 (2019).
55. W. Wang, G. Huang, C. An, S. Zhao, X. Chen and P. Zhang, *J. Clean. Prod.*, **172**, 1986 (2018).
56. L. Y. Lee, S. Gan, M. S. Y. Tan, S. S. Lim, X. J. Lee and Y. F. Lam, *J. Clean. Prod.*, **113**, 194 (2016).
57. S. Kaur, S. Rani and R. K. Mahajan, *J. Chem.*, **2013**, 1 (2013).
58. M. F. Alkhatib, A. A. Mamun and I. Akbar, *Int. J. Environ. Sci. Technol.*, **12**, 1295 (2015).
59. M. Wang, J. Fu, Y. Zhang, Z. Chen, M. Wang, J. Zhu, W. Cui, J. Zhang and Q. Xu, *J. Macromol. Sci. Part A Pure Appl. Chem.*, **52**, 105 (2015).
60. S. N. Jain and P. R. Gogate, *J. Environ. Chem. Eng.*, **5**, 3384 (2017).
61. C. Wang, C. Feng, Y. Gao, X. Ma, Q. Wu and Z. Wang, *Chem. Eng. J.*, **173**, 92 (2011).
62. M. Shirzad-Siboni, A. Khataee, F. Vafaei and S. W. Joo, *Korean J. Chem. Eng.*, **31**, 1451 (2014).
63. R. R. Mohammed and M. F. Chong, *J. Environ. Manage.*, **132**, 237 (2014).
64. G. Ciobanu, M. Harja, L. Rusu, A. M. Mocanu and C. Luca, *Korean J. Chem. Eng.*, **31**, 1021 (2014).
65. M. Shirzad-Siboni, S. J. Jafari, O. Giahi, I. Kim, S. M. Lee and J. K. Yang, *J. Ind. Eng. Chem.*, **20**, 1432 (2014).
66. T. V. Tran, D. T. C. Nguyen, H. T. N. Le, O. T. K. Nguyen, V. H. Nguyen, T. T. Nguyen, L. G. Bach and T. D. Nguyen, *R. Soc. Open Sci.*, **6**, 190058 (2019).
67. F. Fatma, P. L. Hariani, F. Riyanti and W. Sepriani, *Indones. J. Chem.*, **18**, 222 (2018).
68. A. Bhattacharyya, B. Banerjee, S. Ghorai, D. Rana, I. Roy, G. Sarkar, N. R. Saha, S. De, T. K. Ghosh, S. Sadhukhan and D. Chattopadhyay, *Int. J. Biol. Macromol.*, **116**, 1037 (2018).
69. N. Liu, H. Wang, C. H. Weng and C. C. Hwang, *Arab. J. Chem.*, **11**, 1281 (2018).
70. C. Wu, C. Lin, S. Lo and T. Yasunaga, *J. Colloid Interface Sci.*, **208**, 430 (1998).

Supporting Information

Magnetic graphene oxide-biomass activated carbon composite for dye removal

Tan Yan Ying*, Abdul Aziz Abdul Raman*,†, Mustapha Mohammed Bello, and Archina Buthiyappan***

*Department of Chemical Engineering, Faculty of Engineering, University of Malaya, 50603 Kuala Lumpur, Malaysia
**Centre for Dryland Agriculture, Bayero University, P.M.B. 3011, Kano State, Nigeria
(*Received 17 April 2020 • Revised 30 June 2020 • Accepted 7 July 2020*)

Table S1. RSM-CCD with experimental values for adsorption using PKS-AC

Run	pH	Adsorbent dosage (g/L)	Time (h)	Color removal (%)	Adsorption capacity (mg/g)
1	7.0	3.0	4.0	42.9	14.5
2	11.0	1.0	2.0	13.5	16.6
3	3.0	5.0	2.0	67.3	16.6
4	7.0	3.0	4.0	61.5	20.6
5	7.0	3.0	4.0	57.0	19.2
6	11.0	1.0	6.0	2.9	6.4
7	7.0	3.0	6.6	83.0	27.8
8	1.7	3.0	4.0	99.0	33.3
9	7.0	0.4	4.0	16.2	45.4
10	7.0	5.6	4.0	88.3	15.7
11	7.0	3.0	1.4	46.3	15.6
12	11.0	5.0	6.0	90.9	18.3
13	12.3	3.0	4.0	70.1	25.9
14	3.0	1.0	2.0	25.1	60.6
15	3.0	1.0	6.0	31.5	63.8
16	11.0	5.0	2.0	71.3	14.5
17	7.0	3.0	4.0	66.2	22.2
18	7.0	3.0	4.0	76.1	25.5
19	3.0	5.0	6.0	92.5	19.2
20	7.0	3.0	4.0	76.8	25.7

Table S2. RSM-CCD with experimental values for adsorption using GO

Run	pH	Adsorbent dosage (g/L)	Time (h)	Color removal (%)	Adsorption capacity (mg/g)
1	7.0	3.0	4.0	88.2	29.5
2	11.0	1.0	2.0	57.6	59.2
3	3.0	5.0	2.0	70.8	14.2
4	7.0	3.0	4.0	87.8	29.3
5	7.0	3.0	4.0	96.5	32.3
6	11.0	1.0	6.0	46.2	48.3
7	7.0	3.0	6.6	96.2	32.1
8	1.7	3.0	4.0	95.0	32.6
9	7.0	0.4	4.0	26.2	70.9
10	7.0	5.6	4.0	97.4	17.3
11	7.0	3.0	1.4	74.3	24.9
12	11.0	5.0	6.0	99.0	19.9
13	12.3	3.0	4.0	89.5	30.8
14	3.0	1.0	2.0	37.3	67.0
15	3.0	1.0	6.0	31.4	63.7
16	11.0	5.0	2.0	93.7	18.8
17	7.0	3.0	4.0	96.6	32.3
18	7.0	3.0	4.0	96.7	32.3
19	3.0	5.0	6.0	97.4	19.8
20	7.0	3.0	4.0	92.1	30.8

Table S3. RSM-CCD with experimental values for adsorption using MGOAC composite

Run	pH	Adsorbent dosage (g/L)	Time (h)	Color removal (%)	Adsorption capacity (mg/g)
1	7.0	3.0	4.0	96.6	32.2
2	11.0	1.0	2.0	14.2	14.2
3	3.0	5.0	2.0	96.9	19.4
4	7.0	3.0	4.0	96.7	32.2
5	7.0	3.0	4.0	96.1	32.0
6	11.0	1.0	6.0	15.8	15.8
7	7.0	3.0	6.6	97.6	32.5
8	1.7	3.0	4.0	100.0	33.3
9	7.0	0.4	4.0	26.5	72.0
10	7.0	5.6	4.0	100.0	17.8
11	7.0	3.0	1.4	96.3	32.1
12	11.0	5.0	6.0	56.8	11.4
13	12.3	3.0	4.0	28.5	9.5
14	3.0	1.0	2.0	73.0	73.0
15	3.0	1.0	6.0	75.2	75.2
16	11.0	5.0	2.0	55.5	11.1
17	7.0	3.0	4.0	91.5	30.5
18	7.0	3.0	4.0	96.7	32.2
19	3.0	5.0	6.0	98.4	19.7
20	7.0	3.0	4.0	97.5	32.5

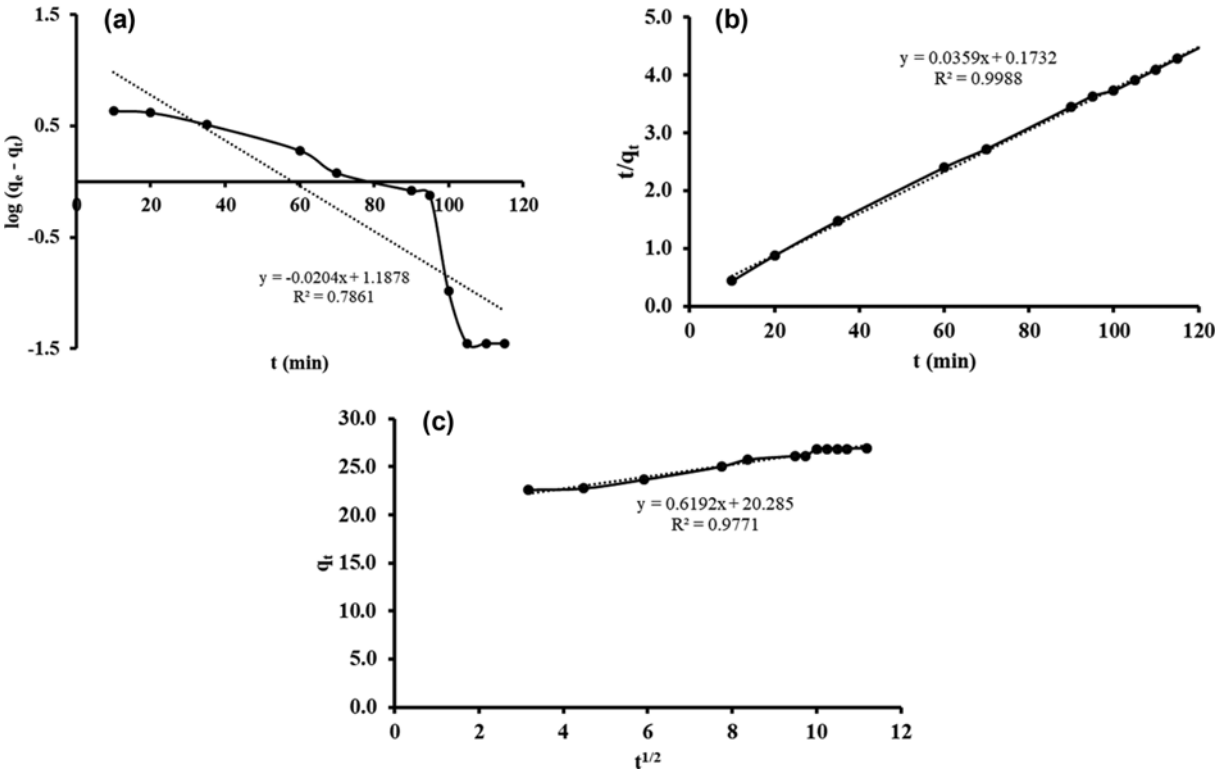

Fig. S1. Kinetic models for (a) pseudo-first-order (b) pseudo-second-order and (c) intra-particle diffusion for adsorption using MGOAC.

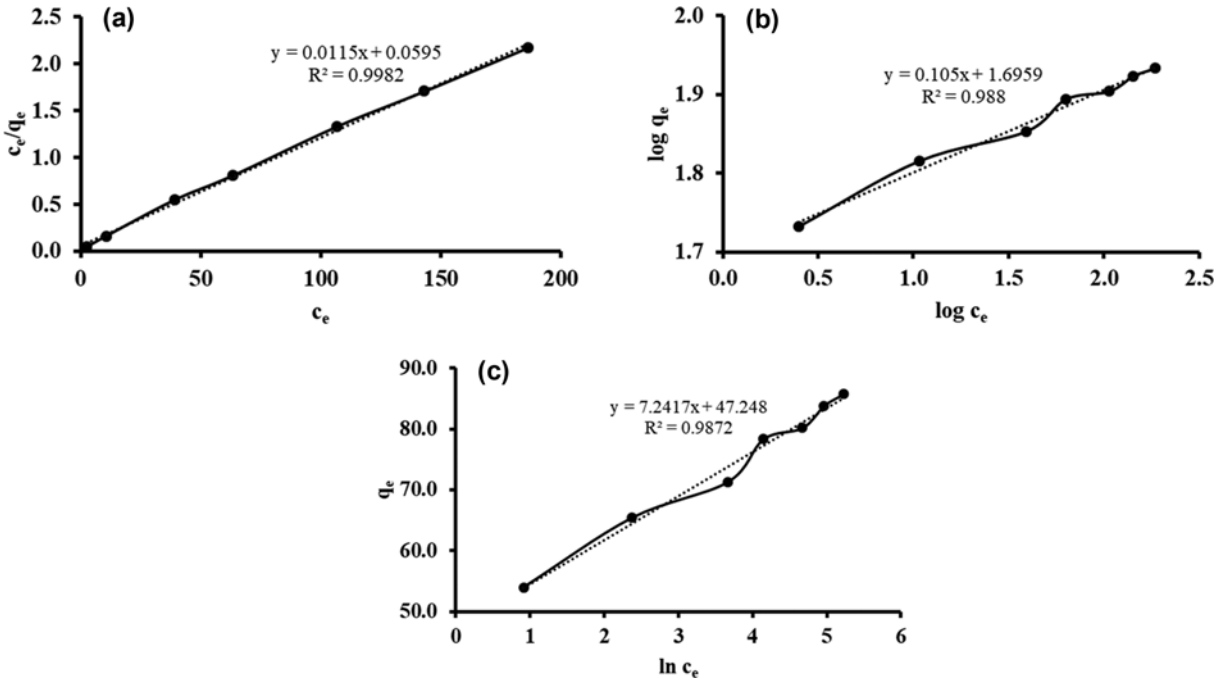

Fig. S2. MGOAC for (a) Langmuir (b) Freundlich and (c) Temkin models.

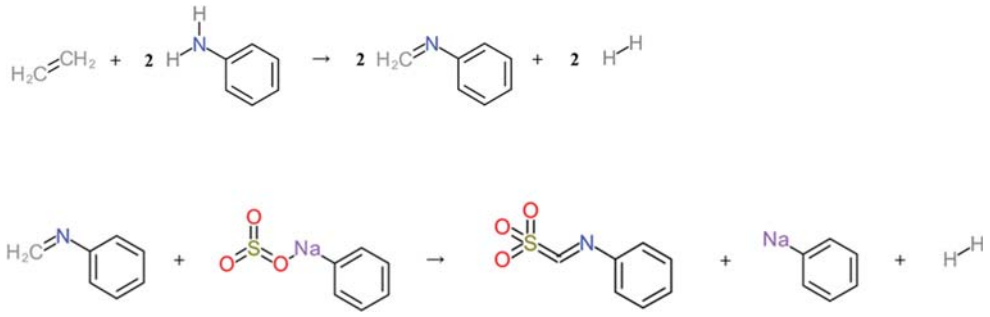

Fig. S3. Plausible adsorption mechanism.